Journal of Pharmaceutical and Biomedical Analysis 156 (2018) 23–35

Contents lists available at ScienceDirect

Journal of Pharmaceutical and Biomedical Analysis

journal homepage: www.elsevier.com/locate/jpba

Chemometrics-assisted investigation of interactions of Tasmar with human serum albumin at a glassy carbon disk: Application to electrochemical biosensing of electro-inactive serum albumin

Ghobad Mohammadi[a], Elahe Faramarzi[b], Majid Mahmoudi[b], Sirous Ghobadi[c], Ali Reza Ghiasvand[d], Hector C. Goicoechea[e], Ali R. Jalalvand[b,*]

[a] Department of Pharmaceutics, School of Pharmacy, Kermanshah University of Medical Sciences, Kermanshah, Iran
[b] Research Center of Oils and Fats, Kermanshah University of Medical Sciences, Kermanshah, Iran
[c] Department of Biology, Faculty of Science, Razi University, Kermanshah, Iran
[d] Department of Chemistry, Lorestan University, Khoramabad, Iran
[e] Laboratorio de Desarrollo Analítico y Quimiometría (LADAQ), Catedra de Química Analítica I, Universidad Nacional del Litoral, Ciudad Universitaria, CC242 (S3000ZAA), Santa Fe, Argentina

ARTICLE INFO

Article history:
Received 2 March 2018
Received in revised form 8 April 2018
Accepted 14 April 2018
Available online 17 April 2018

Keywords:
Tasmar
Human serum albumin
Interaction
Matrix augmentation
Hard modeling
Amperometric biosensing

ABSTRACT

In this work, voltammetric data recorded by a glassy carbon electrode (GCE) was used to investigate the interactions of tolcapone (Tasmar, TAS) with human serum albumin (HSA) at the electrode surface. The recorded voltammetric data was also combined with spectroscopic data to construct an augmented data matrix which was analysed by multivariate curve resolution-alternating least squares (MCR-ALS) as an efficient chemometric tool to obtain more information about TAS-HSA interactions. The results of MCR-ALS confirmed formation of one complex species (HSA-TAS_2) and application of MCR-BANDS to the results of MCR-ALS confirmed the absence of rotational ambiguities and existing unambiguous and reliable results. Binding of TAS to HSA was also modeled by molecular docking and the results showed that the TAS was bound to sub-domain IIA of HSA which were compatible with the ones obtained by recording experimental data. Hard-modeling of combined voltammetric and spectroscopic data by EQUISPEC helped us to compute binding constant of HSA-TAS_2 complex species which was compatible with the binding constant value obtained by direct analysis of experimental data. Finally, a new electroanalytical method was developed based on TAS-HSA interactions for determination of HSA in two ranges of 0–541 nM and 541–1200 nM with a limit of detection of 0.04 nM and a sensitivity of 0.02 $\mu A\,nM^{-1}$.

1. Introduction

In living organisms, there are a vast number of small molecules with various biological and pharmaceutical functions. Tolcapone (Tasmar, TAS, Fig. S1A) with a brand name of Tasmar is a drug which has widespread uses in treatment of Parkinson's disease as an adjunct to levodopa/benserazide or levodopa/carbidopa medications [1]. TAS acts as a potent, selective and reversible nitrocatechol-type inhibitor [1].

Human serum albumin (HSA, Fig. S1B) is the most important protein of human blood plasma which acts as a transport molecule for endogenous and exogenous ligands and foreign molecules including dyes and drugs (small molecules) [2–7]. The HSA has a vital role in free concentration, distribution, metabolism, excretion and interaction with small molecules. Therefore, investigation of interactions of drugs with HSA is very important. On the other side, unusual concentration of HSA in serum or urine is an important biomarker for detection of some diseases such as diabetes, cardiovascular disease, kidney disease, etc. Therefore, developing an efficient, fast and low-cost analytical technique for determination of HSA is of great importance in medicine, biology and diagnostics [8,9].

There are many techniques such as capillary electrophoresis [10], NMR [11], FT-IR [12], UV–vis spectrophotometry [13], HPLC [14] and electrochemistry [15] which can be used to study drug-protein interactions. Some of these methods have been assisted by chemometrics to obtain more reliable information about drug-protein interactions [2–4,16–18]. Chemometrics-assisted investigation of protein-drug interactions can help us to gain

* Corresponding author.
E-mail address: ali.jalalvand1984@gmail.com (A.R. Jalalvand).

https://doi.org/10.1016/j.jpba.2018.04.021
0731-7085/

valuable information about the studied system which cannot be obtained by using conventional methods.

In the present study, electrochemical and spectroscopic data were separately used to investigate the interactions of TAS with HSA and then, electrochemical and spectroscopic data were combined to construct an augmented data matrix and resolved by MCR-ALS to obtain new information about TAS-HSA interactions. The next step of our study was focused on hard-modeling of combined electrochemical and spectroscopic data by EQUISPEC as a hard-modeling chemometric tool to compute binding constant of the complex product. The binding of TAS to HSA was also modeled by molecular modeling techniques to verify the results of experimental sections. Finally, a sensitive electrochemical determination of electro-inactive HSA was performed by two amperometric measurements at the surface of the GCE modified with multiwalled carbon nanotubes-graphene-ionic liquid to develop a new analytical technique for the analysis of protein.

2. Experimental and theoretical considerations

2.1. Chemicals and solutions

HSA (fatty acid-free), TAS, warfarin (Wr), ibuprofen (Ip), ethanol, dimethylformamide (DMF), Tris hydrochloride, 1-ethyl-3-methylimidazolium bis(trifluoromethylsulfonyl)Imide (IL), dimethyl sulfoxide (DMSO), sodium hydroxide, sodium chloride and hydrochloric acid were purchased from Sigma. Multiwalled carbon nanotubes (MWCNTs) were prepared from Ionic Liquid Technologies. Graphene (Gr) was purchased from PubChem. Other chemicals used in this study were purchased from well-known and legal companies and used as received without any further purification. A Tris buffer solution (TBS) with a concentration of 0.05 M containing 0.025 M sodium chloride to maintain the ionic strength was prepared to control pH at 7.4. Stock solutions of TAS and HSA with a concentration of 0.1 M were prepared in the TBS (0.05 M, pH 7.4) and kept in a refrigerator. Stock solutions of Wr and Ip with a concentration of 0.1 M were prepared in DMSO and kept in a refrigerator. Working solutions used in this study were prepared from their stock solutions by appropriate dilutions. 50 mg MWCNTs was dissolved in 1 mL DMF and 100 μL IL and 50 mg Gr were also added to it and ultrasonicated for 30 min to obtain a homogeneous MWCNTs-Gr-IL solution. Doubly distilled water (DDW) was used to prepare all the solutions used in this study.

Three human serum samples were prepared from a medical diagnostic laboratory and 10 mL of each sample was centrifuged at 4500 rpm for 20 min and after discarding the supernatants, 5 mL of each sample was diluted with 45 mL TBS (0.05 M, pH 7.4). Then, each samples was amperometrically analysed towards HSA determination and final concentration of HSA in serum samples was calculated by applying appropriate dilution factors.

2.2. Instruments and softwares

The electrochemical data of this study was recorded by an Autolab (PGSTAT302N-high performance) controlled by the NOVA software (version 2.1.2). The Autolab was equipped by an electrochemical cell in which a bare or modified GCE, a Pt wire and an Ag/AgCl electrode acted as working, counter and reference electrode, respectively. The SEM images were captured by a KYKY-EM 3200 scanning electron microscope. Spectrofluorimetric data were recorded by a Cary Eclipse fluorescence spectrophotometer equipped with a water bath and a 1.0 cm quartz cell. Spectrophotometric data were recorded by an Agilent 8453 UVvis Diode-Array spectrophotometer controlled by the Agilent UVvis ChemStation software and equipped with a 1.0 cm quartz cell. A sigma centrifuge was used to centrifuge the serum samples. An ELMEIRON pH-meter (CP-411) was used to pH adjustments. The molecular structure of the TAS was constructed by Hyperchem package (Version 8.0) and AM1 semi empirical method with Polak-Ribiere algorithm was used to minimize energy until the root mean square gradient of 0.01 kcal mol^{-1}. The known crystal structure of HSA (PDB Id: 1AO6) was downloaded from Brookhaven Protein Data Bank (PDB) and water molecules were removed from its PDB file and hydrogen atoms were added to it. The Molegro virtual docker (MVD) software was used to generate a docked conformation of TAS with HSA. LIGPLOT which is a well-known program for automatically plotting protein-ligand interactions [19], was used to plot the interactions between TAS and HSA. The m-files of MCR-ALS and MCR-BANDS were downloaded from internet [20]. The recorded experimental data was transferred to MATLAB (Version 7.14) environment and smoothed, when necessary. To accelerate exact computing concentrations of TAS, HSA and their ratio during voltammetric or spectroscopic titrations, a simple homemade MATLAB program was written.

2.3. Fabrication of the modified electrodes

Prior to the modification of the GCE, it was well polished with a silky polishing pad and rinsed with DDW. It was then immersed into a beaker containing ethanol and ultrasonicated for 30 min and finally rinsed with DDW and covered until analysis time. To fabricate HSA/GCE, 10 μL HSA (0.01 M) was dropped onto the surface of the cleaned GCE and left to be dried at room temperature. To fabricate MWCNTs-Gr-IL/GCE, 10 μL MWCNTs-Gr-IL was dropped onto the surface of the cleaned GCE and left to be dried at room temperature. Fig. 1A–C shows the SEM images captured from the surface of bare GCE, HSA/GCE and MWCNTs-Gr-IL/GCE, respectively. By comparing Fig. 1A and B, it can be clearly observed that HSA has formed a layer on the surface of bare the GCE. Fig. 1C shows that tubes of CNTs and sheets of Gr which have been attached onto the surface of the electrode.

2.4. Experiments required to construct an augmented data matrix for the analysis by MCR-ALS

Experiment 1 ($\boldsymbol{D}_{DPV}^{TAS}$): HSA in the range of 0.0–5.0 × 10^{-5} M was added to a solution with a constant concentration of TAS at 5.0 × 10^{-5} M.

Experiment 2 ($\boldsymbol{D}_{DPV}^{HSA}$): TAS in the range of 0.0–5.0 × 10^{-5} M was added to a solution with a constant concentration of HSA at 1.0 × 10^{-5} M.

Experiment 3 ($\boldsymbol{D}_{LSV}^{TAS}$): HSA in the range of 0.0–5.0 × 10^{-4} M was added to a solution with a constant concentration of TAS at 5.0 × 10^{-4} M.

Experiment 4 ($\boldsymbol{D}_{LSV}^{HSA}$): TAS in the range of 0.0–5.0 × 10^{-4} M was added to a solution with a constant concentration of HSA at 1.0 × 10^{-4} M.

Experiment 5 ($\boldsymbol{D}_{CV}^{TAS}$): HSA in the range of 0.0–5.0 × 10^{-4} M was added to a solution with a constant concentration of TAS at 5.0 × 10^{-4} M.

Experiment 6 ($\boldsymbol{D}_{CV}^{HSA}$): TAS in the range of 0.0–5.0 × 10^{-4} M was added to a solution with a constant concentration of HSA at 1.0 × 10^{-4} M.

Experiment 7 ($\boldsymbol{D}_{F}^{TAS,298.15}$): HSA in the range of 0.0–1.0 × 10^{-7} M was added to a solution with a constant concentration of TAS at 1.0 × 10^{-7} M.

Experiment 8 ($\boldsymbol{D}_{F}^{HSA,298.15}$): TAS in the range of 0.0–5.0 × 10^{-7} M was added to a solution with a constant concentration of HSA at 1.0 × 10^{-7} M.

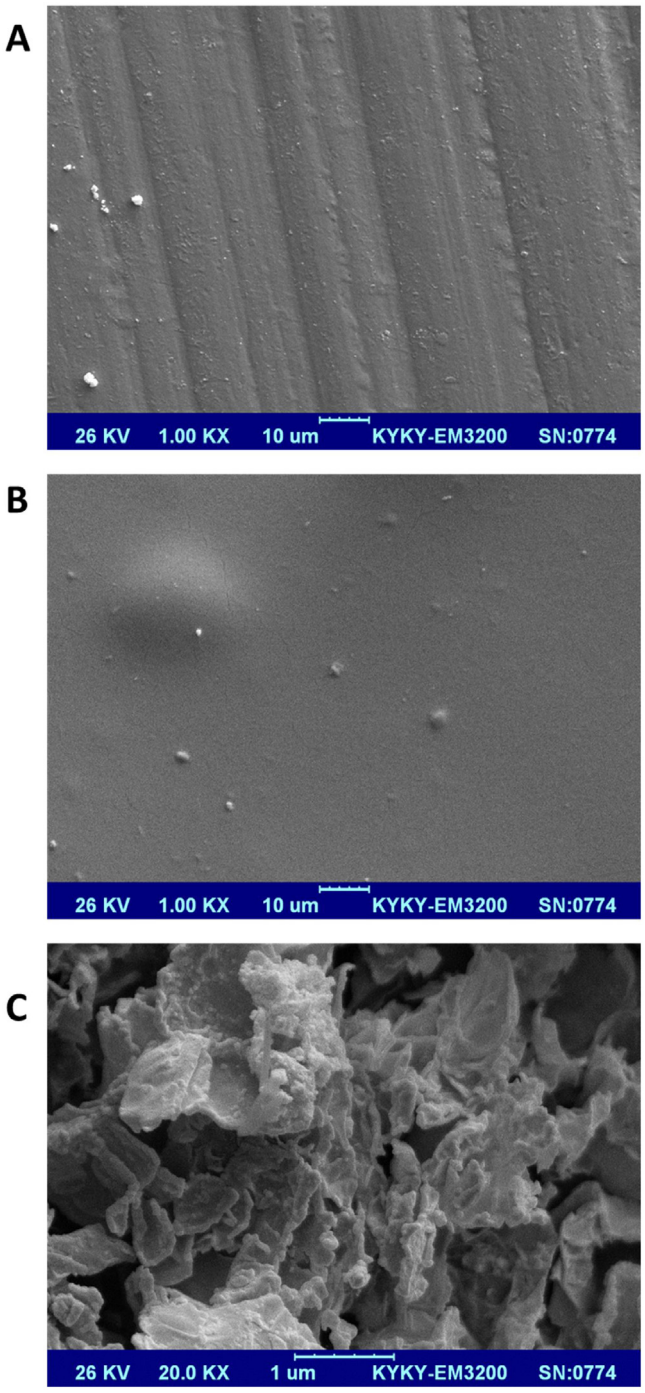

Fig. 1. SEM images captured from the surface of (A) bare GCE, (B) HSA/GCE and (C) MWCNTs-Gr-IL/GCE.

All the experimental data matrices have been coded and described in Table S1.

2.5. Requirements for applying MCR-ALS to the augmented data matrix

There are some reports on foundations for applying MCR-ALS to the analysis of electroanalytical data [21,22]. Here, we are going to describe a summary of required information. MCR is able to decompose a recorded voltammetric or spectroscopic data matrix ($\boldsymbol{D}$ (M × N), M objects and N variables e.g. wavelength or potential) into the different pure profiles for each component of a mixture. The extracted information for pure components is in the form of single bands or more complex profiles. Decomposition of a data matrix ($\boldsymbol{D}$) by MCR is performed according to the following equation:

$$\boldsymbol{D} = \boldsymbol{C}\boldsymbol{S}^{T} + \boldsymbol{E} \quad (1)$$

where matrix $\boldsymbol{C}$ (M × P) contains the concentration profiles of the P species, matrix $\boldsymbol{S}^{T}$ (P × N) contains the pure signals' profiles and matrix $\boldsymbol{E}$ ($M \times N$) contains residuals. ALS is one of the most important iterative approaches used to solve Eq. (1). Start of optimization process needs initial guesses of $\boldsymbol{C}$ and $\boldsymbol{S}^{T}$ and these initials will be then refined to obtain meaningful profiles.

When a chemical system is studied using more than one instrumental technique, a column- and row-wise augmented data matrix is constructed which will be decomposed by MCR-ALS. In the present study, we have studied TAS-HSA interactions by differential pulse voltammetry (DPV), linear sweep voltammetry (LSV), cyclic voltammetry (CV) and fluorescence spectroscopy (F) and individual data matrices corresponding to the mentioned techniques were placed side-by-side as shown below:

$$\begin{bmatrix} \boldsymbol{D}_{DPV}^{TAS}\boldsymbol{D}_{LSV}^{TAS}\boldsymbol{D}_{CV}^{TAS}\boldsymbol{D}_{F}^{TAS,298.15} \\ \boldsymbol{D}_{DPV}^{HSA}\boldsymbol{D}_{LSV}^{HSA}\boldsymbol{D}_{CV}^{HSA}\boldsymbol{D}_{F}^{HSA,298.15} \end{bmatrix} = \begin{bmatrix} \boldsymbol{C}^{TAS} \\ \boldsymbol{C}^{HSA} \end{bmatrix} \left[\boldsymbol{S}_{DPV}^{T}\boldsymbol{S}_{LSV}^{T}\boldsymbol{S}_{CV}^{T}\boldsymbol{S}_{F}^{T}\right] + \left[\boldsymbol{E}_{DPV}\boldsymbol{E}_{LSV}\boldsymbol{E}_{CV}\boldsymbol{E}_{F}\right] \quad (2)$$

$\boldsymbol{D}_{DPV}$, $\boldsymbol{D}_{LSV}$, $\boldsymbol{D}_{CV}$ and $\boldsymbol{D}_{F}$ contain the data recorded by DPV, LSV, CV and F techniques. $\boldsymbol{C}^{TAS}$ and $\boldsymbol{C}^{HSA}$ are row-wise augmented data matrices containing measured profiles and $\boldsymbol{S}^{T}_{DPV}$, $\boldsymbol{S}^{T}_{LSV}$, $\boldsymbol{S}^{T}_{CV}$ and $\boldsymbol{S}^{T}_{F}$ contain the pure signals.

Evolving Factor Analysis (EFA) or Principal Component Analysis (PCA) as efficient methods can be applied to determine the number of species (P) of the augmented data matrix [23]. The EFA method is able to provide an initial estimation of changing concentration of the species during the experiment based on the evaluation of the magnitude of the eigenvalues associated with all the submatrices of the augmented data matrix. EFA performs calculations in forward and reversed direction of the experiments [24]. PCA is a well-known chemometric tool which yields the number of species in a bilinear data set [25]. During ALS optimization some constraints are implemented which facilitate the finding of representative contributions to the data matrix and to ensure that the final solution is chemically meaningful or not [26]. The resolution is started with initial estimates of $\boldsymbol{C}$ which iteratively optimizes the concentration by applying the available information about the system [25]. The lack of fit (*lof*) is the difference between the input data ($\boldsymbol{D}$) and the data obtained by MCR-ALS which is used as a criterion to evaluate the goodness of fit of the model and is calculated according to the following equation [27]:

$$lof\,(\%) = 100\sqrt{\frac{\sum_{i,j} e_{i,j}^{2}}{\sum_{i,j} d_{i,j}^{2}}} \quad (3)$$

where d_{ij} refers to an element in the raw data and e_{ij} is its corresponding residual.

The solutions applied to Eq. (1) by MCR-ALS are not unique and may have some ambiguities such as rotational and intensity ambiguities and column- and row-wise augmentation which was described in Eq. (2) can be used to tackle this challenge. This type of data analysis which enables us to simultaneous analysis of different types of data is more powerful than that described by Eq. (1) and can help us for resolution of a very complex data matrix. Furthermore, this method may be useful to overcome small signal shifts observed in the data as well. Therefore, we constructed an augmented data matrix for resolution by MCR-ALS. However, because of combining different types of data, the following considerations have been considered in the analysis of the augmented data matrix:

1. Voltammetric data have much higher intensity than spectroscopic data therefore, all the submatrices were divided by their maximum values to normalize them and to have similar weight on the iterative ALS optimization and then used to construct the augmented data matrix.
2. Because of having different types of data, the concept of component is more complicated here. From spectroscopic point of view, a component is a pure chemical species in solution [28,29], but from electrochemical point of view, a component is not only associated to a single electrochemical process which gives a signal, but also is associated with the other possible phenomena such as adsorption at the electrode surface or capacitive currents [21,22].
3. For augmentation of voltammetric and spectroscopic matrices to construct an augmented matrix, all the matrices should have the same number of rows and columns and also must have the same distribution of the species during experiments. To achieve this condition, TAS and HSA must have the same total concentrations in all titrations, but achieving to this condition is not possible because voltammetric experiments need higher concentrations than spectroscopic experiments. Therefore, we performed all the voltammetric and spectroscopic experiments at different total concentrations but with the same values of ratio.

3. Results and discussion

3.1. Voltammetric studies of TAS-HSA interactions

3.1.1. Cyclic voltammetry

CV is a powerful method which could be applied to monitor small molecule-protein interactions [30]. Therefore, it was applied to investigate TAS-HSA interactions and to achieve this goal, HSA in the range of 0.0–5.0 × 10^{-4} M was added to a solution with a constant concentration of TAS at 5.0 × 10^{-4} M, and the related CVs were recorded which are shown in Fig. S2A. The first CV (curve a) is related to TAS in the absence of HSA and upon addition of HSA (curves b-u) its peak current and peak potential were decreased and increased, respectively, which were related to the changes of the molecular environment around the TAS molecule and its interactions with HSA [31]. These phenomena also confirmed that TAS is interacted with the hydrophobic region of the HSA cavity [32,33]. E_p (peak potential) and $E_{p/2}$ (half-peak potential) values of the CV of TAS at the surface of GCE are 180 and 130 mV, respectively, and according to $|E_p - E_{p/2}| = 47.7/\alpha n$ [34] which describes an irreversible oxidation at the electrode surface, where n is the electron transfer number and α is assumed to be 0.5 for an irreversible electrode process [35], n was calculated to be 1.90 i.e. ~ 2.

Binding of a small molecule to a biomacromolecule may affects the electrochemical kinetic parameters of the small molecule including α (transfer coefficient) and k_s (electrochemical rate constant). Therefore, to investigate the changes in α and k_s of TAS due to its binding with HSA, the CVs of TAS at the surface of GCE (free TAS) and HSA/GCE (TAS bound to HSA) were recorded at different scan rates (25–750 mV s^{-1}) and the results are showing in Figs. S2B and C, respectively. A linear dependence between peak currents and scan rates was observed for TAS at the surface of bare GCE (free TAS) and HSA/GCE (TAS bound to HSA) which revealed that TAS oxidation at the surface of both electrodes was an adsorption-controlled process (Figs. S2D and E). Furthermore, according to Eq. (4) [36], the surface concentrations (Γ) of the electroactive species including free TAS (Γ_{TAS}) and TAS-HSA ($\Gamma_{TAS\text{-}HSA}$) can be calculated from the slopes of the plots depicted in Figs. S2D and E, respectively.

$$I = n^2F^2A\Gamma\upsilon/4RT \quad (4)$$

where n is the number of electrons (two electron), A is the surface area of the GCE (0.05 cm^2), T is temperature and Γ (mol cm^{-2}) is the surface coveraged. According to the information mentioned above, Γ_{TAS} and $\Gamma_{TAS\text{-}HSA}$ were calculated to be 9.83 × 10^{-5} and 1.07 × 10^{-4} mol cm^{-2}, respectively. Laviron's equation (Eq. (5)) [37], can express the relationship between E_P and υ for a totally irreversible electrochemical reaction:

$$E_p = E^0\text{-}2.3RT/\alpha nF[\log(RTK_s/nF)\text{-}\log\upsilon] \quad (5)$$

where E^0 (V) was the formal potential, and other symbols have their conventional meaning. If the E^0 is known, by plotting E_p against log υ, the intercept and the slope of the plot give k_s and α values, respectively. The E^0 can be calculated from the intercept of E_p vs. υ plot (Fig. S2F, curves *a* and *b*). According to the slopes of curves *a* and *b* of Fig. S2G, the α values for free TAS and TAS bound to HSA were calculated to be 0.556 and 0.297, respectively and according to the intercepts of curves *a* and *b* of Fig. S2G, the k_s values for free TAS and TAS bound to HSA were calculated to be 1.982 and 1.05 × 10^{-3}, respectively. As can be seen, the values of α and k_s values were decreased in the presence of HSA. Decrease in α may be due to higher absorption of TAS-HSA complex at the electrode surface and decrease in k_s may be attributed to the lower rate of electron transfer of TAS in the form of TAS-HSA complex.

Immobilization of a biomacromolecule onto the surface of the GCE can help us to obtain information about the type of interaction of small molecule with the biomacromolecule [38,39]. Therefore, the CVs of TAS at bare GCE and HSA/GCE were recorded and are shown in Fig. 2A. As can be seen, oxidation peak potential of TAS was shifted to more positive potentials at the surface of HSA/GCE. As reported by the other researchers [38], positive shifts in peak potential of TAS at the surface of HSA/GCE revealed that the interaction of TAS with HSA occurred through hydrophobic forces.

Fig. 2 The CV was also used to investigate the binding of TAS to HSA/GCE by recording the CVs of TAS at different concentrations on the surface of HSA/GCE (not shown). The current of the CVs were increased with increasing concentration of TAS (C_{TAS}) and then reached to saturation values which was according to the shape of Langmuir adsorption. According to Eq. (6) [40], where I, I_{max}, and K_b are the peak intensity, maximum peak intensity, and the binding constant of TAS at HSA/GCE surface, respectively, by the regression of C_{TAS}/I on C_{TAS}, the K_b value was calculated to be 5.81 × 10^5 mol^{-1} L.

$$C_{TAS}/I = (1/K_bI_{max}) + (C_{TAS}/I_{max}) \quad (6)$$

3.1.2. Linear sweep and differential pulse voltammetry

The LSVs and DPVs of TAS in the presence of increasing concentration of HSA in the TBS (0.05 M, pH 7.4) were recorded at the surface of GCE and the results are shown in Fig. 2B and C, respectively. The results showed that the peak current of TAS was decreased and shifted to more positive potentials upon addition of HSA. Such a phenomenon may be related to the interaction of TAS with HSA and its embedding within the HSA structure which decreases the equilibrium concentration of TAS in solution or occurrence of a competitive adsorption occurred at the electrode surface. When a biomacromolecule such as hemoglobin or serum albumin or DNA with a low concentration is interacted with a small molecule, only a low area of the electrode surface (10%) is covered which indicates a very little competitive adsorption of small molecules at the electrode surface [41]. However, another probability maybe existed which maybe related to the possible unfolding of the HSA structure by increasing TAS concentration which provides some pathways for TAS to access the tryptophan or tyrosine residues of the HSA and subsequently oxidation at the GCE surface [42]. But, we think that multivariate resolution of the measured

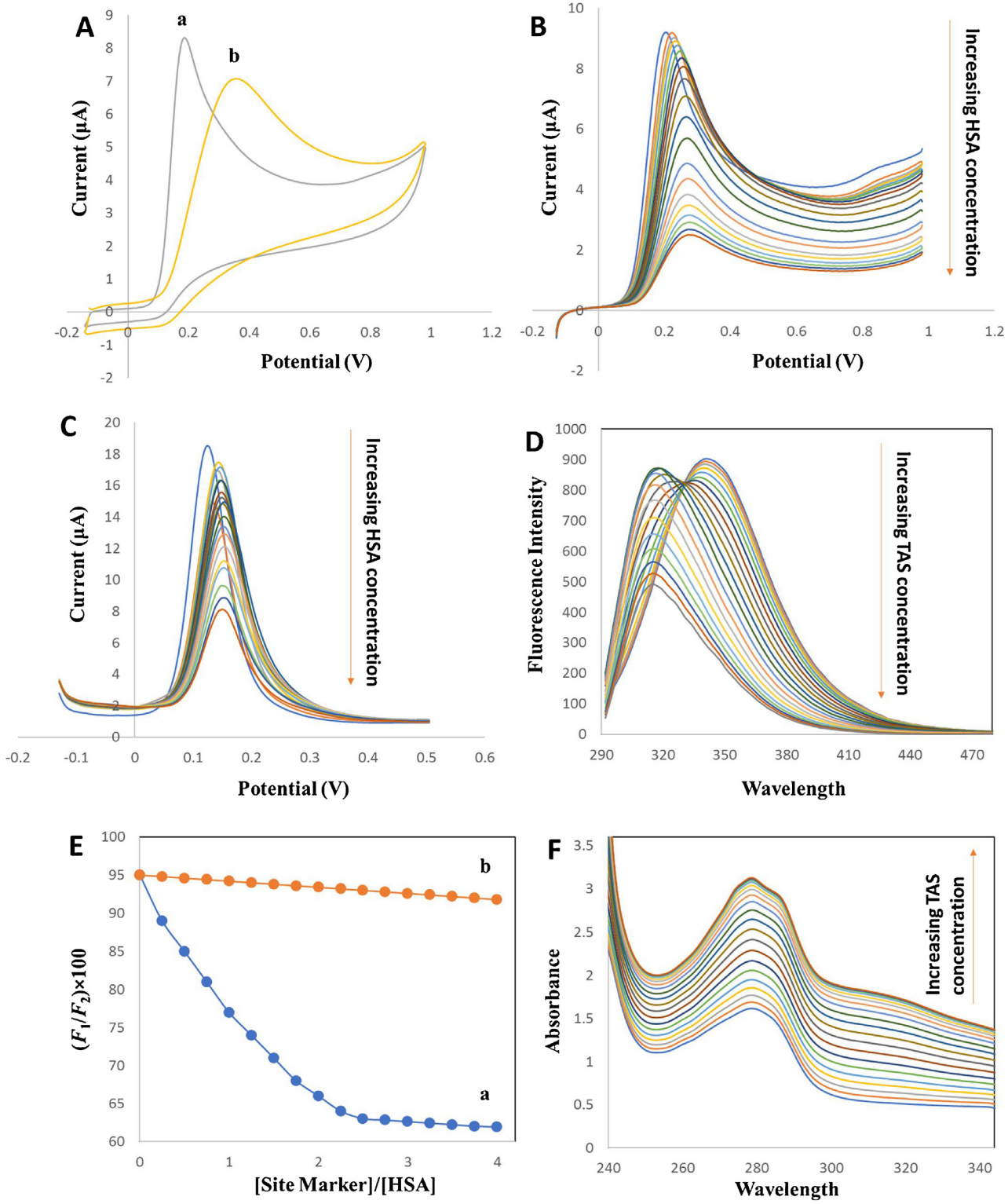

Fig. 2. (A) CVs of 5.0×10^{-4} M TAS prepared in the TBS (0.05 M, pH 7.4) recorded at the surface of the bare GCE (curve a) and HSA/GCE (curve b), (B) LSVs of 5.0×10^{-4} M TAS prepared in the TBS (0.05 M, pH 7.4) in the presence of increasing concentration of HSA in the range of 0.0–5.0×10^{-4} M, (C) DPVs of 5.0×10^{-5} M TAS prepared in the TBS (0.05 M, pH 7.4) in the presence of increasing concentration of HSA in the range of 0.0–5.0×10^{-5} M, (D) fluorescence spectra of 1.0×10^{-6} M HSA prepared in the TBS (0.05 M, pH 7.4) upon increasing concentration of TAS in the range of 0.0-5.0×10^{-6} M, λ_{ex} = 280 nm, (E) effects of Wr (curve a) and Ip (curve b) as site markers on the fluorescence of HSA-TAS and (F) UvVis absorption spectra of 1.0×10^{-7} M HSA prepared in the TBS (0.05 M, pH 7.4) in the presence of increasing concentration of TAS in the range of 0.0–5.0×10^{-7} M.

Table 1
Stern-Volmer quenching constants at different temperatures related to TAS-HSA interactions.

T (K)	K_{SV} ($\times 10^5$ L mol^{-1})	R^2
298.15	5.11	0.999
304.15	4.74	0.998
310.15	4.08	0.999

profiles is needed to obtain more information about the occurrence of the phenomena mentioned above.

3.2. Spectroscopic studies of TAS-HSA interactions

3.2.1. Spectrofluorimetry

The fluorescence emission spectra of HSA with a concentration of 1.0×10^{-7} M prepared in the TBS (0.05 M, pH 7.4) in the presence of increasing concentration of TAS in the range of 0.0-5.0 $\times 10^{-7}$ M were recorded at three different temperatures (i.e., 298.15, 304.15 and 310.15 K) and one of them (298.15 K) is shown in Fig. 2D. As can be seen, the fluorescence intensity of HSA was gradually decreased upon increasing TAS concentration. HSA has a single tryptophan residue (Trp-214) and its intrinsic fluorescence in the UV region is related to this residue. When a small molecule is interact with HSA, the Trp fluorescence intensity is changed by decreasing the quantum yield of fluorescence [43]. Different molecular interactions such as molecular rearrangements, energy transfer, excited state reactions, ground state complex formation, and collisional quenching can cause fluorescence quenching. But, the mechanisms of quenching are usually included dynamic collision and static quenching (complex formation). Stern-Volmer equation is usually used to describe the fluorescence quenching [44]:

$$F_0/F = 1 + K_{SV}[Q] \tag{7}$$

where F_0 and F refer to the steady-state fluorescence intensities in the absence and presence of the quencher (TAS), respectively. K_{SV} and $[Q]$ are the Stern-Volmer quenching constant and concentration of the quencher, respectively. According to Eq. (7), F_0/F values were regressed on concentrations of TAS (not shown) and the results are presented in Table 1. As can be seen, the K_{SV} values were decreased with increasing temperature which suggested a static quenching (complex formation) for quenching of fluorescence emission of HSA by TAS.

3.2.2. Site selectivity of binding of TAS to HSA

HSA has two sites including site I (hydrophobic sub-domain IIA) [45] and Sudlow's sites II (sub-domain IIIA) [46] which enable small molecules to bind with HSA. To identify the binding site location of TAS on HSA, two competitive experiments were carried out by two site markers including Wr (marker of site I) and Ip (marker of site II). In these experiments, Wr or Ip was added in the range of 0.0-8.0 $\times 10^{-7}$ M to a binary mixture of TAS and HSA where TAS concentration (2.0×10^{-7} M) was four times higher than HSA (5.0×10^{-8} M). Then, $(F_1/F_2) \times 100$ where F_1 and F_2 are the fluorescence intensity in the absence and presence of site marker, respectively, was plotted against [Site Marker]/[HSA], Fig. 2E. The changes induced by the site markers enabled us to understand the binding location of TAS on HSA. As can be seen, by the addition of Wr to the HSA-TAS solution the $(F_1/F_2) \times 100$ was decreased gradually (Fig. 2E, curve a) which confirmed that the binding of TAS to HSA was affected by the addition of Wr. While, $(F_1/F_2) \times 100$ was not affected by the addition of Ip (Fig. 2E, curve b) which indicated that the Ip did not prevent the usual binding location of TAS on HSA. The results discussed above showed that Wr competed with TAS molecules while Ip did not. Therefore, the binding site of TAS was mainly located in hydrophobic pocket in sub-domain IIA of HSA.

3.2.3. Spectrophotometry

UvVis spectrophotometric titration was also used to investigate the interaction of TAS with HSA. Spectrophotometric titration of HSA with a constant concentration of 1.0×10^{-6} M prepared in the TBS (0.05 M, pH 7.4) upon increasing concentration of TAS in the range of 0.0–5.0 $\times 10^{-6}$ M was performed and the related spectra were recorded in the range of 240–340 nm which are shown in Fig. 2F. As can be seen, HSA has an absorbance peak at 280 nm which its position and intensity were affected in the presence of TAS. By the addition of TAS into HSA solution, the absorption at 280 nm was gradually increased (hyperchromism) which maybe related to interactions of TAS with HSA.

3.2.4. Energy transfer from HSA to TAS and measurement of the binding distance

Fluorescence energy transfer (FRET) is a general spectroscopic technique which is used to measure molecular distance in biological systems [47]. The efficiency (E, Eq. (8)) of FRET depends on some factors such as the inverse sixth power of the distance between donor and acceptor (r) which must be within 2–8 nm (Forster distance) [48], Forster radius (R_0, Eq. (9)) or the critical energy transfer distance, overlapping of emission of donor and absorption of acceptor and orientation of the transition dipole of the donor.

$$E = 1 - \frac{F}{F_0} = \frac{R_0^6}{\left(R_0^6 + r^6\right)} \tag{8}$$

$$R_0^6 = 8.8 \times 10^{-25} k^2 n^{-4} J \Phi \tag{9}$$

In Eqs. (8–9), k^2, n, Φ and J are spatial factor of orientation, refractive index of the medium, fluorescence quantum yield of the donor and the overlap integral of the fluorescence emission spectrum for the donor and the absorption spectrum of the acceptor, respectively. The J can be calculated by the following equation:

$$J = \frac{\int_\infty {}^0 F(\lambda)\,\varepsilon(\lambda)\,\lambda^4 d\lambda}{\int_\infty {}^0 F(\lambda)\,d\lambda} \tag{10}$$

where $F(\lambda)$ and ε are the fluorescence intensity of the donor and molar absorption coefficient of the acceptor at the wavelength λ, respectively. The values of k^2, n and Φ are 2/3, 1.336 and 0.118, respectively [49], and according to these values, the values of J, R_0, E and r were calculated to be 5.4×10^{-14} cm^3 M^{-1}, 3.24 nm, 0.012 and 6.84 nm, respectively. As can be seen, r is less than 8 nm which confirms that the energy can be transferred from HSA to TAS with high probability [50].

3.3. Combining voltammetric and spectroscopic data

3.3.1. Justification of the MCR-ALS results

In order to further investigation of interactions of TAS with HSA for obtaining more information about any HSA-TAS$_m$ (m is referred to the number of TAS contributed in complex formation with HSA) complex and the relative concentrations of the various reactant and product species, multivariate analysis of the recorded experimental data was performed by MCR-ALS as an efficient chemometric tool. To achieve this goal, a column- and row-wise augmented data matrix was constructed by arranging eight individual data matrices obtained by DPV ($\boldsymbol{D}_{DPV}^{TAS}$, Fig. 2C, $\boldsymbol{D}_{DPV}^{HSA}$, Fig. 3A), LSV ($\boldsymbol{D}_{LSV}^{TAS}$, Fig. 2B, $\boldsymbol{D}_{LSV}^{HSA}$, Fig. 3B), CV ($\boldsymbol{D}_{CV}^{TAS}$, Fig. S2A, $\boldsymbol{D}_{CV}^{HSA}$, Fig. 3C) and F ($\boldsymbol{D}_{F}^{TAS}$, Fig. 3D, $\boldsymbol{D}_{F}^{HSA}$, Fig. 2D) and then, the MCR-ALS was used to the analysis of the augmented data matrix.

Fig. 3 The first step was focused on application of singular value decomposition (SVD) to the augmented data matrix for determination of the number of species and here, the SVD detected three main components. One may guess that these three components

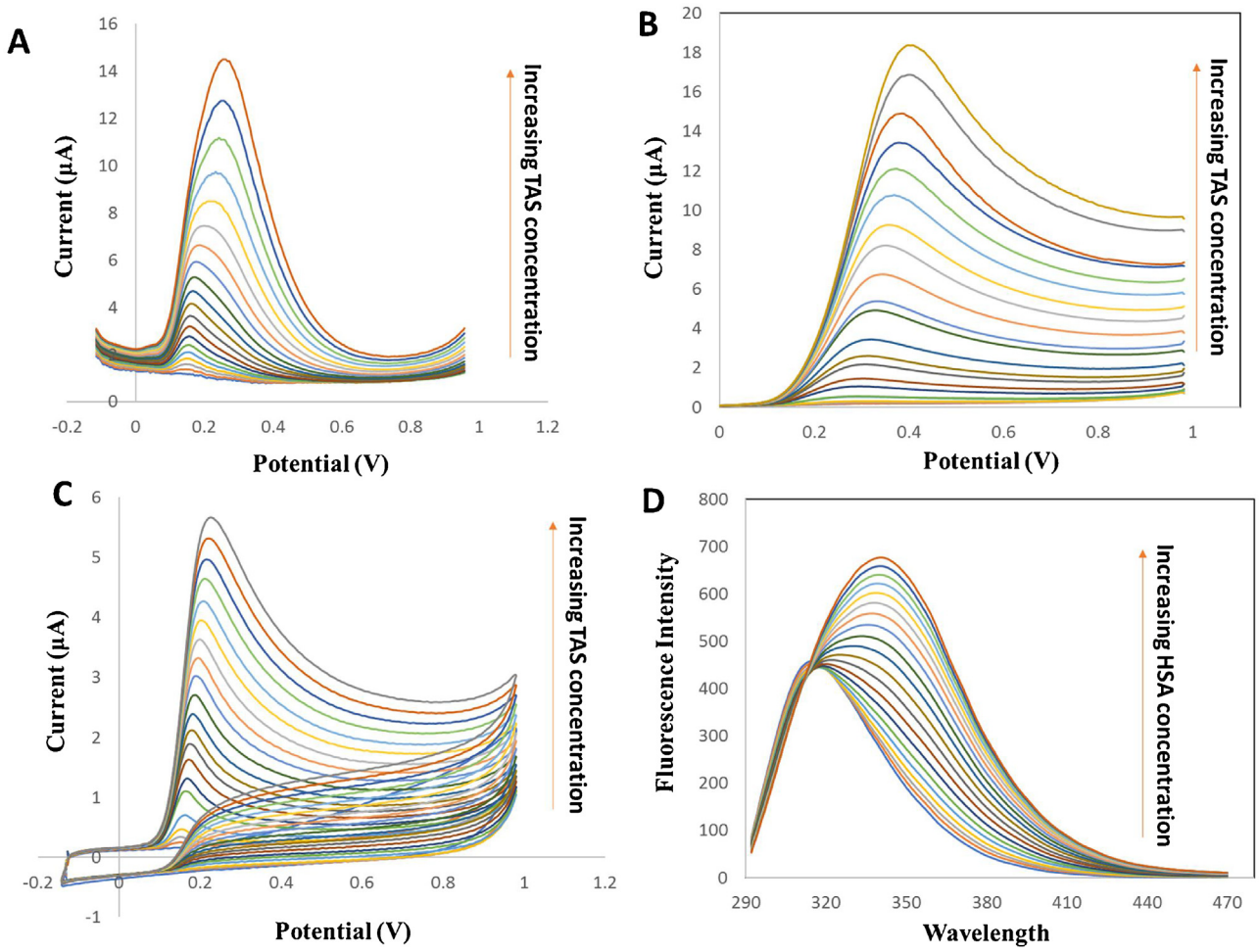

Fig. 3. (A) DPVs of 1.0×10^{-5} M HSA in the presence of increasing concentration of TAS in the range of 0.0–5.0×10^{-5} M, (B) and (C) LSVs and CVs of 1.0×10^{-4} M HSA in the presence of increasing concentration of TAS in the range of 0.0–5.0×10^{-4} M, respectively, and (D) fluorescence emission spectra of 1.0×10^{-7} M TAS in the presence of increasing concentration of HSA in the range of 0.0–1.0×10^{-7} M, λ_{ex} = 280 nm.

are related to free drug (TAS), free HSA and one HSA-TAS_m complex species. The second step was focused on finding an initial estimate of the concentration profiles of the involved species by the use of EFA. The EFA has been basically designed for working with full rank data sets and its straightforward application to the analysis of the rank-deficient data matrix cannot provide useful information. This challenge was tackled by the method introduced by de Juan et al. based on matrix augmentation [51]. Comparing with the other iterative methods such as iterative target transformation factor analysis (ITTFA), the MCR-ALS has an important advantage which is including application of some constraints to the data matrix in iteration process resulting in obtaining more reliable results. It should be noted that due to the presence of the CV data matrices in the augmented data matrix which contain negative and positive values, the non-negativity constraint was only applied to the concentration profiles. Application of a closure constraint to the matrices obtained at different concentration levels is not possible.

With the conditions mentioned above, the ALS optimization was started on the MCR results. As previously mentioned, the *lof* which is the difference between the input data ($\boldsymbol{D}$) and the data reproduced from the product ($\boldsymbol{CS}^T$) obtained by MCR-ALS was used as a parameter to evaluate the goodness of fit of the model. In this work, 7.13% was found as the best *lof* value which explained almost all of the variability in the experimental data presented as a product of the extracted signals and the concentration profiles.

The results of MCR-ALS are showing in Fig. 4A–F. Fig. 4A and B show the concentration profiles of the species involved in experiments. Fig. 4A shows that when HSA is added to TAS, concentration of TAS is decreasing and a new complex species is forming. As can be seen, the concentration of the complex species is reached equilibrium at the ratio of [HSA]/[TAS] ~ 0.5 which shows this species is a HSA-TAS_2 complex species. Fig. 4B shows that at the ratio of [TAS]/[HSA] ~ 2 concentrations of HSA and TAS are sharply decreased and increased, respectively, which confirms the most intensity of complex formation is occurred at this ratio and also confirms that the complex species is HSA-TAS_2. Therefore, according to the results of SVD and resolved concentration profiles, we can conclude that three species are involved in titration process which are belonging to the free TAS, free HSA and a HSA-TAS_2 complex species. The pure voltammetric and spectral profiles resolved by MCR-ALS are shown in Fig. 4C–F which provide new qualitative information about the nature of the species involved in each technique. From voltammetric profiles we can conclude that HSA is not electroactive while the complex species is electroactive. The resolved voltammograms of HSA suggested that the HSA in its original structural format was electro-inactive, while the extracted voltammograms for the complex species showed that it was electroactive. Accessibility of the potentially oxidizable tryptophan and tyrosine side chain residues is necessary for being electroactive, and this will be facilitated by unfolding the HSA structure upon reacting

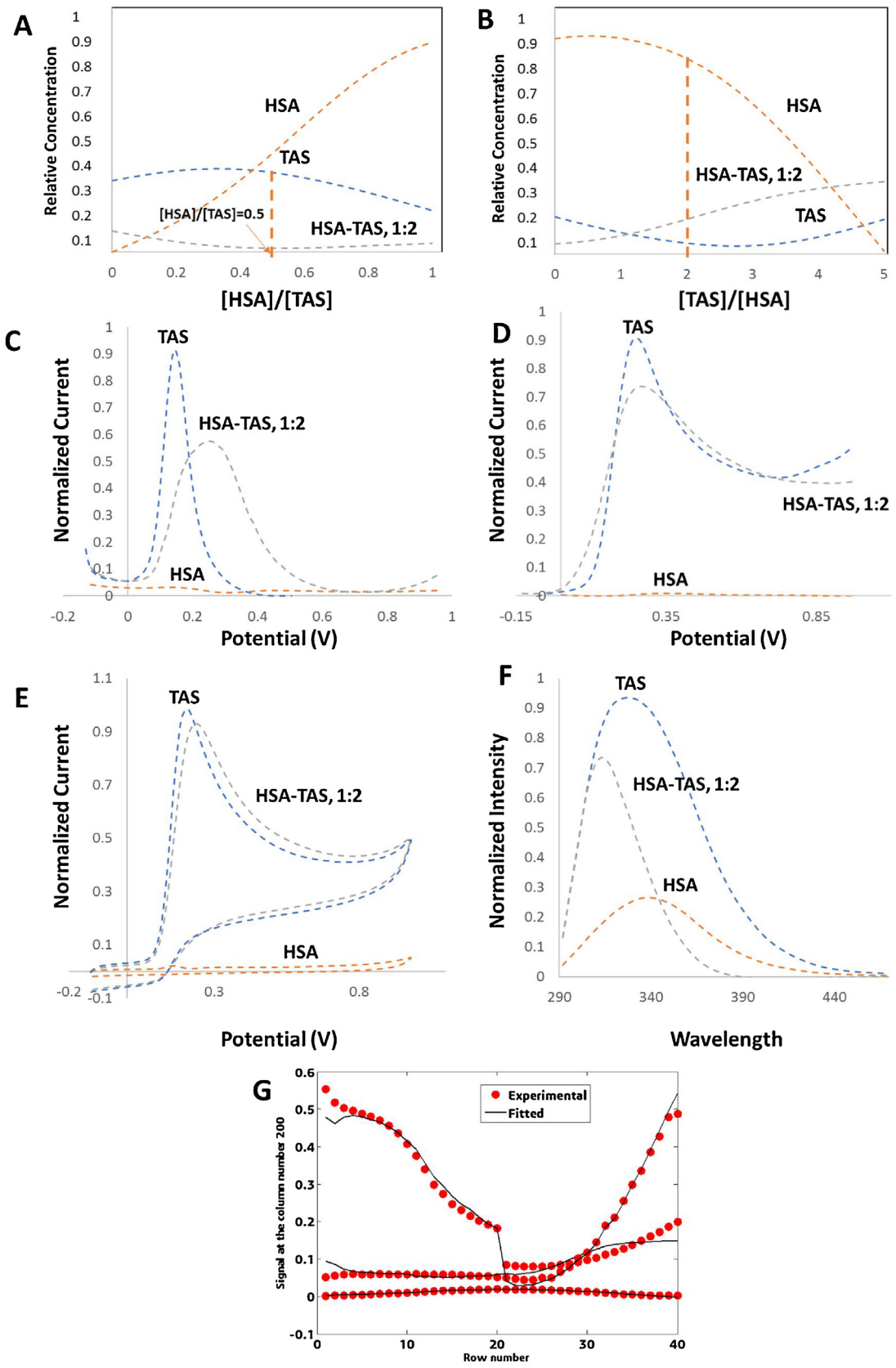

Fig. 4. The results of applying MCR-ALS to the augmented data matrix for simultaneous resolution of voltammetric and spectroscopic data: (A) and (B) extracted concentration profiles of species involved, (C)–(F) extracted signals of different species involved in DPV, LSV, CV and F experiments, respectively, and (G) plot of coinciding experimental (points) and calculated data (line).

with TAS. Therefore, it can be suggested that the locating of two TAS molecules within HSA structure facilitates the unfolding of the HSA structure which causes tryptophan and tyrosine side chain residues to be accessible for oxidation at the electrode surface. The plot with coincided experimental and theoretical data which has been shown in Fig. 4G is a strong evidence for high quality of the fitting process.

In order to further investigation of the stoichiometry of the complex species formed during TAS-HSA interactions, the mole-ratio method was also applied to the recorded experimental data as shown in Fig. S3. As can be seen, the curves were inflected at [TAS]/[HSA] ~ 2 which confirmed formation of HSA-TAS_2 complex species upon interactions of TAS with HSA which also confirmed the results of the multivariate analysis of the augmented data matrix by MCR-ALS.

3.3.2. Verification of the existence of ambiguities in MCR-ALS results by MCR-BANDS

One of the most important advantages of MCR rather than the other bilinear methods is natural constraints which help it to have physical meaningful solution [52]. However, in some cases, instead of a unique solution, a band of feasible solutions can be applied which causes ambiguities in the solution of MCR [53]. Therefore, an important thing in applying MCR is finding a unique and meaningful solution to interpret the experimental data. MCR-BANDS as an efficient chemometric tool was introduced to calculate maximum and minimum of the relative contribution of the components to estimate the feasible solutions [52,54]. MCR-BANDS is a good method to provide an estimation of the extent of rotational ambiguity [55].

Here, the MCR-BANDS was used to verify the existence of rotational ambiguities in the results of MCR-ALS. To achieve this goal, MCR-BANDS with the same constraints used in MCR-ALS was applied to the data matrix obtained by MCR-ALS. The maximum relative contribution function (f^{max}) and minimum relative contribution function (f^{min}) for each contributing species including HSA ($f^{max} = 0.244$ and $f^{min} = 0.244$), TAS ($f^{max} = 0.301$ and $f^{min} = 0.301$) and HSA-TAS_2 ($f^{max} = 0.412$ and $f^{min} = 0.412$) were computed and fortunately, for all the contributing species there is no difference between the f^{max} and f^{min} which confirm that there is no rotational ambiguity [52]. The absence of rotational ambiguity is related to matrix augmentation and resolution by applying suitable constraints.

3.4. Hard-modeling of experimental data

In hard-modeling methods, a model including stoichiometry of the species and an estimation of binding constant value is defined which can be applied to the decomposition of data matrix $\boldsymbol{D}$ according to Eq. (1). The model defined is used to obtain an estimation of the concentration profiles ($\boldsymbol{C}$) and then, least squares fitting is used to obtain the pure spectra ($\boldsymbol{S}^T$) with best matching of $\boldsymbol{C}$ and $\boldsymbol{D}$. The differences between the data in $\boldsymbol{D}$ and the reproduced data matrix are collected in a residual data matrix ($\boldsymbol{E}$). The hard-modeling algorithm continues the optimization procedure by tuning the stoichiometry of the proposed species until a desired level of residuals $\boldsymbol{E}$ is reached. To obtain more information about mathematical details of the hard-modeling, the reader is referred to Ref. [56].

In our work, EQUISPEC as a hard-modeling approach was applied to an augmented data matrix built by combining spectroscopic and voltammetric data to calculate the binding constants with the aim of verifying the results of Section 3.1.1. The calculated binding constants are presented in Table S2. Interestingly, the results of EQUISPEC are in a good agreements with those reported in Section 3.1.1.

3.5. Molecular docking

In this study, the MVD software was applied to understand the binding mode of TAS at the HSA. Docking of TAS to HSA was performed via MolDock as a docking module and MolDock SE as a search algorithm and the number of runs was set to 10. A population size of 50 and a maximum iteration of 1500 was used for parameter settings. The maximum number of poses generated was 10. Fig. 5A–C shows TAS bound to HSA with different views. After docking the TAS with HSA, the binding sites were detected which included Trp 214, Leu 219, Lys 199, Leu 238, Arg 257, Arg 222, Leu 260, Ile 264, Ile 290, Lys 195, Glu 153, Tyr 150, Glu 292, Ala 291 and Ala 261. The ΔG for the binding of TAS to HSA was obtained as $-24.01\ kJ\ mol^{-1}$. As can be seen, TAS has bound to sub-domain IIA of HSA which also conforms the results of Section 3.2.2. The LIGPLOT program was also used to more explore interactions between TAS and HSA as shown in Fig. 5D. Two hydrogen bond between TAS and Arg 222 (2.39 and 3.17 Å), one hydrogen bond between TAS and Arg 257 (3.01 Å) and one hydrogen bond between TAS and Lys 195 (2.47 Å) were observed, and Ala 291, Glu 292, Tyr 150, Lys 199, Leu 238, Ile 264, Leu 260, and Ile 290 had hydrophobic interactions with TAS. The hydrophobic interactions were also detected by the results of the Section 3.1.1.

3.6. Analytical characterizations

Here, we are going to develop a novel analytical method based on TAS-HSA interactions for highly sensitive determination of HSA, and because of higher sensitivity of amperometric methods than voltammetric ones, amperometric sensing of HSA was preferred. In order to increase the sensitivity of the developed methodology, we decided to use a modified GCE instead of bare GCE. Therefore, the bare GCE was modified with MWCNTs-Gr-IL (Fig. 1C) and used as the biosensing platform in amperometric measurements.

3.6.1. Amperometric measurements

In amperometric measurements, the MWCNTs-Gr-IL/GCE, a Pt wire and Ag/AgCl electrode were acted as working, counter and reference electrode, respectively. Here, because of electro-inactivity of HSA two different amperometric measurements including in the absence and presence of HSA were performed for determination of HSA. The first amperometric measurement was performed by immersing the MWCNTs-Gr-IL/GCE into a cell containing 10 mL TBS (0.05 M, pH 7.4) as supporting electrolyte which was gently stirred at 1000 rpm. Then, thirteen different concentrations of TAS ranging in 1–45 μM were injected into the cell solution upon applying a potential of 0.05 V (oxidation potential of TAS at the surface of MWCNTs-Gr-IL/GCE) and the related *i*-*t* values were collected by the NOVA software and depicted in Fig. 6A. In second amperometric measurement, TAS with the same concentrations used for the first measurement but in the presence of increasing concentration of HSA in the range of 0.1–1200 nM was injected to the cell solution for thirteen times and the related i^*-*t* values were collected by the NOVA software and depicted in Fig. 6B. To construct a calibration curve for sensing of HSA, $\Delta i = i\text{-}i^*$ values were regressed on concentrations of HSA as shown in Fig. 6C. As can be seen, two linear ranges of 0–541 nM and 541–1200 nM were obtained for the biosensing of HSA. The sensitivity and limit of detection (LOD) of the sensor were calculated to be $0.02\ \mu A\ nM^{-1}$ and 0.04 nM respectively. The LOD was calculated according to $3SD/m$, where *SD* is the standard deviation of the intercept and *m* is the slope of the calibration curve.

3.6.2. Interference study

The selectivity of the developed sensor for determination of 200 nM HSA in the presence of 200-fold concentration of cysteine, tyrosine, histidine, valine, methionine, proline, pheny-

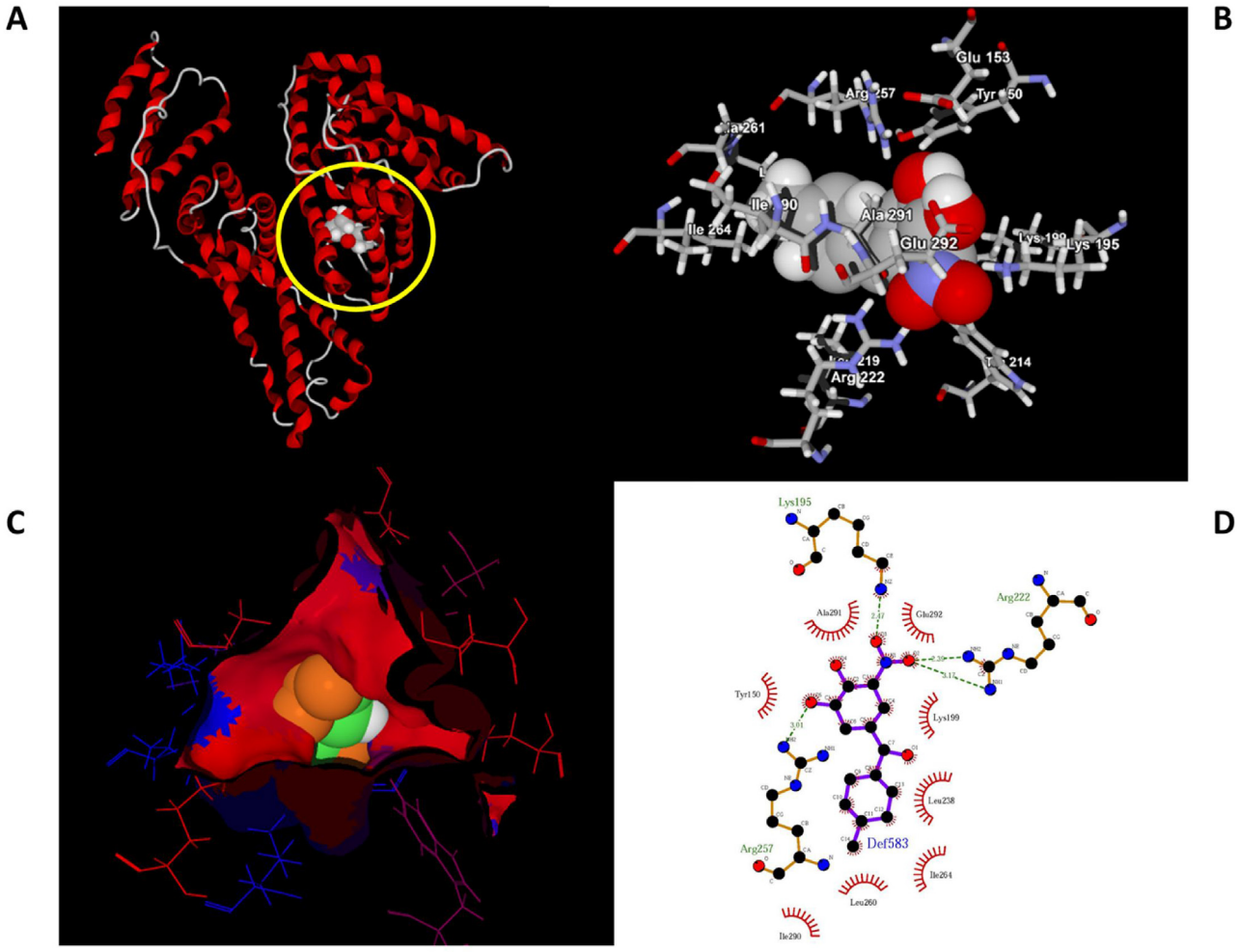

Fig. 5. Computer-generated models of binding TAS to HSA presented by: (A) secondary structure view, (B) pose organizer view and (C) hydrophobicity view. (D) TAS-HSA interactions presented by LigPlot program.

lalanine, egg albumin, chloramphenicol, amoxicillin, vitamin C, vitamin B12, NO_2^-, Zn^{2+}, Sn^{2+} and Ca^{2+} was amperometrically examined and the results are shown in Fig. 6D. As can be seen, the sensor was able to selective determination of HSA even in the presence of high concentrations of interfering species.

3.6.3. Stability, repeatability, and reproducibility

Long-term stability is one of the most important characteristics of an electrochemical sensor which must be verified prior to its application to real samples. Therefore, to verify this parameter, the MWCNTs-Gr-IL/GCE was used to determine 200 nM HSA prepared in the TBS (0.05 M, pH 7.4) by weekly recording of its amperometric response during six weeks and the results are shown in Fig. 6E. As can be seen, the sensor was able to retain 96.2% of its original response which confirmed that the sensor has a good stability. The sensor was also applied to determine 200 nM HSA for ten times during one day and the results showed a good relative standard deviation (RSD) value of 2.31% which confirmed that he sensor response was repeatable. The next study of this section was devoted to the examination of the reproducibility of the fabricated sensor. To achieve this goal, eight sensors were fabricated and separately used to determine 200 nM HSA, and an acceptable value of 3.11% for RSD confirmed that the response of the biosensor was reproducible.

Table 2
Results of the analysis of human serum samples by the reference method and proposed method in this study.

Sample	The proposed method in this study	The reference method
Serum 1	$6.24\ (\pm0.02) \times 10^{-4}$ M	$6.41\ (\pm0.03) \times 10^{-4}$ M
Serum 2	$7.96\ (\pm0.04) \times 10^{-4}$ M	$8.06\ (\pm0.04) \times 10^{-4}$ M
Serum 3	$8.11\ (\pm0.03) \times 10^{-4}$ M	$8.08\ (\pm0.02) \times 10^{-4}$ M

3.6.4. Validation of the developed method

In this section, the performance of the sensor for determination of HSA in human serum samples was examined and the results were compared with those of obtained by a medical diagnostic laboratory whose method was based on capillary electrophoresis (reference method). The results of the analysis of serum samples by the reference method and the method developed in this study are presented in Table 2. As can be seen, there is an acceptable agreement between the results obtained by the two methods. But, in comparison with the reference method, the proposed sensor is fast, simple and low-cost. Therefore, accurate determination of HSA in real samples may allow one to propose the present sensor as a low-cost, promissory and accessible alternative for the clinical analysis of protein.

4. Conclusion

In this study, interactions of TAS with HSA were investigated by electrochemical and spectroscopic methods and also in combina-

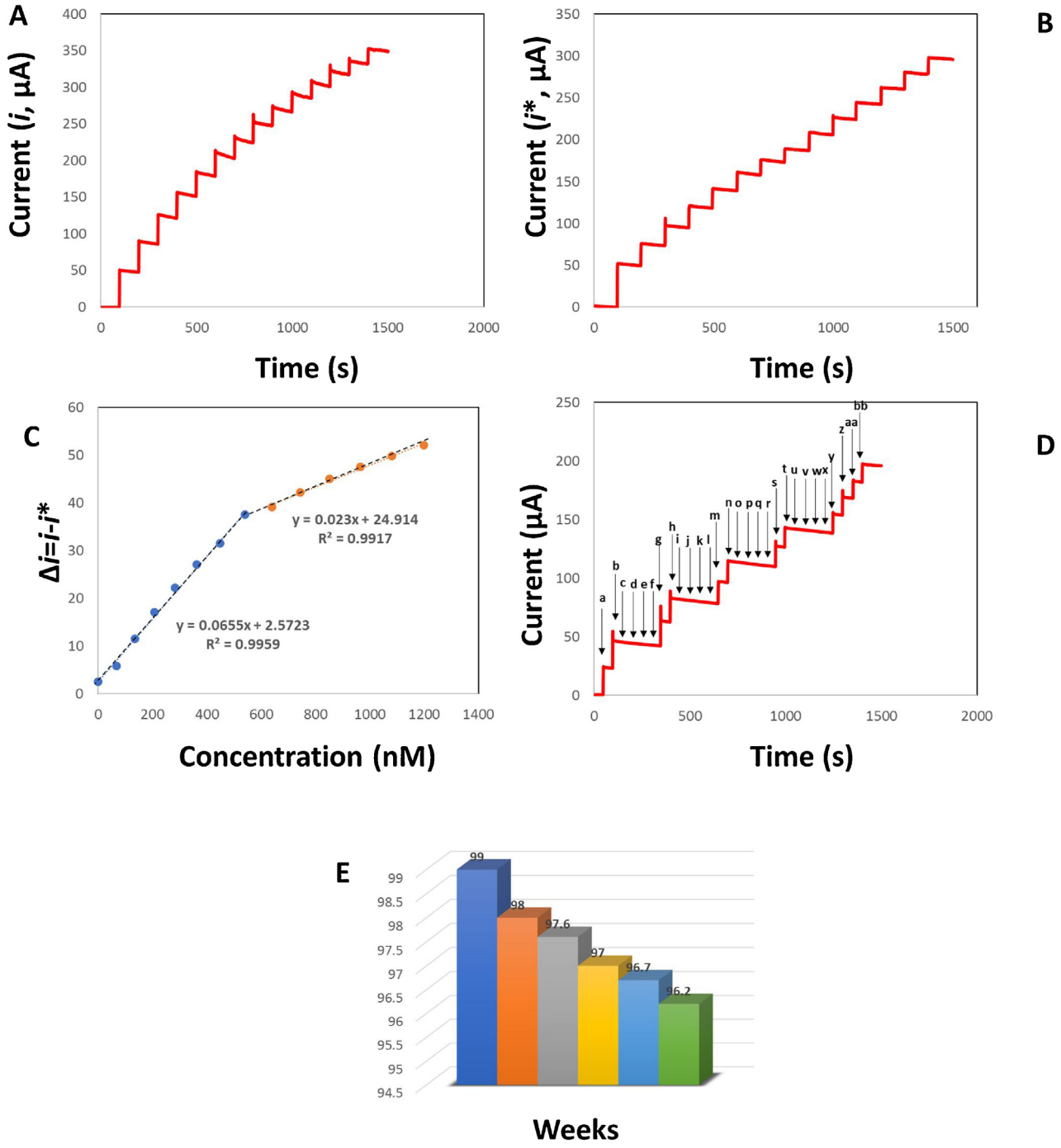

Fig. 6. (A) Amperometric responses recorded by MWCNTs-Gr-IL/GCE upon increasing concentration of TAS from 1 to 45 µM and applying a potential of 0.05 V while the solution was gently stirred at 1000 rpm (B) same as (A) but, in the presence of increasing concentration of HSA in the range of 0.1–1200 nM, (C) regression of $\Delta i = i\text{-}i^*$ values on concentrations of HSA, (D) amperometric responses of the sensor to HSA (a (200 nM), b (200 nM), g (100 nM), h (100 nM), m (100 nM), n (100 nM), s (100 nM), t (100 nM), y (100 nM), z (100 nM), aa (100 nM) and bb (100 nM)) and 200-fold interfering species including (c) cysteine, (d) tyrosine, (e) histidine, (f) valine, (i) methionine, (j) proline, (k) phenylalanine, (l) egg albumin, (o) chloramphenicol, (p) amoxicillin, (q) vitamin C, (r) vitamin B12, (u) NO_2^-, (v) Zn^{2+}, (w) Sn^{2+} and (x) Ca^{2+} and (E) examination of the stability of the sensor response to 200 nM HSA by weekly measurement of its response during six weeks.

tion with each other by chemometric methods. At the first stage of the study, electrochemical and spectroscopic techniques were separately used to obtain some information and then, combined and simultaneously analysed by MCR-ALS as an efficient chemometric tool. The binding of TAS to HSA causes a series of changes in electrochemical and spectral recordings which confirm the interactions between TAS and HSA. The resolved profiles by MCR-ALS were in a good agreements with measured responses which confirmed the successfulness of MCR-ALS in resolving the augmented data matrix. The binding of TAS to HSA was also modeled by molecular docking methods which showed the location of binding of TAS at HSA and the residues interacted with TAS. The results of molecular docking confirmed that TAS is located in sub-domain IIA of HSA which confirmed the results of experimental sections as well. Finally, two amperometric measurements of TAS in the absence and presence of HSA were performed to develop a novel method

for determination of HSA. Fortunately, the developed method was able to determine HSA in serum samples which its results were in a good agreement with those of obtained by a reference method. But, in comparison with the reference method, the proposed sensor is fast, simple and low-cost. Therefore, accurate determination of HSA in real samples may allow one to propose the present sensor as a low-cost, promissory and accessible alternative for the clinical analysis of protein.

Acknowledgment

Hereby, we appreciate the financial supports of this project by Research Council of Kermanshah University of Medical Sciences.

Appendix A. Supplementary data

Supplementary data associated with this article can be found, in the online version, at https://doi.org/10.1016/j.jpba.2018.04.021.

References

[1] https://en.wikipedia.org/wiki/Tolcapone.
[2] M.B. Gholivand, A.R. Jalalvand, H.C. Goicoechea, M. Omidi, Investigation of interaction of nuclear fast red with human serum albumin by experimental and computational approaches, Spectrochim. Acta 115 (Part A) (2013) 516–527.
[3] M.B. Gholivand, A.R. Jalalvand, H.C. Goicoechea, R. Gargallo, T. Skov, Chemometrics: an important tool for monitoring interactions of vitamin B7 with bovine serum albumin with the aim of developing an efficient biosensing system for the analysis of protein, Talanta 132 (2015) 354–365.
[4] M.B. Gholivand, A.R. Jalalvand, H.C. Goicoechea, Multivariate analysis for resolving interactions of carbidopa with dsDNA at a fullerene-C60/GCE, Int. J. Biol. Macromol. 69 (2014) 369–381.
[5] M.B. Gholivand, A.R. Jalalvand, H.C. Goicoechea, T. Skov, Fabrication of an ultrasensitive impedimetric buprenorphine hydrochloride biosensor from computational and experimental angles, Talanta 124 (2014) 27–35.
[6] M.B. Gholivand, A.R. Jalalvand, H.C. Goicoechea, Developing a novel computationally designed impedimetric pregabalin biosensor, Electrochim. Acta 133 (2014) 123–131.
[7] M.B. Gholivand, A.R. Jalalvand, G. Paimard, H.C. Goicoechea, T. Skov, R. Farhadi, S. Ghobadi, N. Moradi, V. Nasirian, Fabrication of a novel naltrexone biosensor based on a computationally engineered nanobiocomposite, Int. J. Biol. Macromol. 70 (2014) 596–605.
[8] C.S. Mahon, D.A. Fulton, Mimicking nature with synthetic macromoleculescapable of recognition, Nat. Chem. 6 (2014) 665–672.
[9] P. Zahedi, M. Ziaee, M. Abdouss, A. Farazin, B. Mizaikoff, Biomacromoleculetemplate-based molecularly imprinted polymers with an emphasis on theirsynthesis strategies: a review, Polym. Adv. Technol. 27 (2016) 1124–1142.
[10] Q.H. Lu, C.D. Ba, D.Y. Chen, Investigating noncovalent interactions of rutin-serum albumin by capillary electrophoresis –frontal analysis, J. Pharm. Biomed. Anal. 47 (2008) 888–891.
[11] B. Bojko, A. Sulkowska, M. Maciazek-Jurczyk, J. Rownicka, W.W. Sulkowski, Investigations of acetaminophen binding to bovine serum albumin in the presence of fatty acid: fluorescence and 1H NMR studies, J. Mol. Struct. 924–926 (2009) 332–337.
[12] J.S. Mandeville, E. Froehlich, H.A. Tajmir-Riahi, Study of curcumin and genistein interactions with human serum albumin, J. Pharm. Biomed. Anal. 49 (2009) 468–474.
[13 Y.Y. Yue, X.G. Chen, J. Qin, X.J. Yao, Characterization of the mangiferin–human serum albumin complex by spectroscopic and molecular modeling approaches, J. Pharm. Biomed. Anal. 49 (2009) 753–759.
[14] C. Bertucci, V. Andrisano, R. Gotti, V. Cavrini, Use of an immobilised human serum albumin HPLC column as a probe of drug–protein interactions: the reversible binding of valproate, J. Chromatogr. B 768 (2002) 147–155.
[15] H.X. Luo, Y. Du, Z.X. Guo, Electrochemistry of N-n-undecyl-N′-(sodium-p-aminobenzenesulfonate) thiourea and its interaction with bovine serum albumin, Bioelectrochemistry 74 (2009) 232–235.
[16] Y.N. Ni, S.S. Wang, S. Kokot, Fluorescence spectrometric study on the interactions of Isoprocarb and sodium 2-isopropylphenate with bovine serum albumin, Anal. Chim. Acta 663 (2010) 139–146.
[17] Y.N. Ni, G.L. Liu, S. Kokot, Fluorescence spectrometric study on the interactions of Isoprocarb and sodium 2-isopropylphenate with bovine serum albumin, Talanta 76 (2008) 513–521.
[18] A.D. Juan, S.C. Rutan, R. Tauler, D.L. Massart, Comparison between the direct trilinear decomposition and the multivariate curve resolution-alternating least squares methods for the resolution of three-way data sets, Chemom. Intell. Lab. Syst. 40 (1998) 19–32.
[19] A.C. Wallace, R.A. Laskowski, J.M. Thornton, LIGPLOT: a program to generate schematic diagrams of protein-ligand interactions, Protein Eng. 8 (1995) 127–134.
[20] http://www.ub.es/gesq/mcr/mcr.htm.
[21] M. Esteban, C. Arino, J.M. Dıaz-Cruz, M.S. Diaz-Cruz, R. Tauler, Multivariate curve resolution with alternating least squares optimisation: a soft-modelling approach to metal complexation studies by voltammetric techniques, Trends Anal. Chem. 19 (2000) 49–61.
[22] M. Esteban, C. Arino, J.M. Dıaz-Cruz, Chemometrics for the analysis of voltammetric data, Trends Anal. Chem. 25 (2006) 86–92.
[23] H. Gampp, M. Maeder, C.J. Meyer, A.D. Zuberbühler, Calculation of equilibrium constants from multiwavelength spectroscopic data—III: model-free analysis of spectrophotometric and ESR titrations, Talanta 32 (1985) 1133–1139.
[24] H. Abdollahi, V. Mahdavi, Tautomerization equilibria in aqueous micellar solutions: A spectrophotometric and factor-analytical study, Langmuir 23 (2007) 2362–2368.
[25] S. Perez, M.J. Culzoni, G.G. Siano, M.D. Gil Garcia, H.C. Goicoechea, M.M. Galera, Detection of unintended stress effects based on a metabonomic study in tomato fruits after treatment with carbofuran pesticide. capabilities of MCR-ALS applied to LC-MS three-way data arrays, Anal. Chem. 81 (2009) 8335–8346.
[26] M. Vives, R. Gargallo, R. Tauler, Study of the intercalation equilibrium between the polynucleotide poly(adenylic)-poly(uridylic) acid and the ethidium bromide dye by means of multivariate curve resolution and the multivariate extension of the continuous variation and mole ratio methods, Anal. Chem. 71 (1999) 4328–4337.
[27] C.B. Zachariassen, J. Larsen, F. Van den Berg, R. Bro, A. De Juan, R. Tauler, Comparison of PARAFAC2 and MCR-ALS for resolution of an analytical liquid dilution system, Chemom. Intell. Lab. Syst. 83 (2006) 13–25.
[28] R. Tauler, A. Izquierdo-Ridorsa, E. Casassas, Simultaneous analysis of several spectroscopic titrations with self-modelling curve resolution, Chemom. Intell. Lab. Syst. 18 (1993) 293–300.
[29] R. Tauler, A.K. Smilde, B.R. Kowalski, Selectivity local rank, three-way data analysis and ambiguity in multivariate curve resolution, J. Chemom. 9 (1995) 31–58.
[30] R.N. Goyal, A.B. Toth, G. Dryhurst, N.T. Nguyen, A comparison of the peroxidase-catalyzed and electrochemical oxidation of uric acid, Bioelectrochem. Bioenerg. 9 (1982) 39–60.
[31] Y. Ni, X. Zhang, S. Kokot, Spectrometric and voltammetric studies of the interaction between quercetin and bovine serum albumin using warfarin as site marker with the aid of chemometrics, Spectrochim. Acta A 71 (2009) 1865–1872.
[32] Q. Zhang, Y. Ni, S. Kokot, Combined voltammetric and spectroscopic analysis of small molecule-biopolymer interactions: the levodopa and serum albumin system, Talanta 88 (2012) 524–532.
[33] S.S. Kalanur, J. Seetharamappa, U. Katrahalli, Voltammetric and spectroscopic investigations on the mechanism of interaction of buzepide methiodide with protein, Colloids Surf. B: Biointerfaces 75 (2010) 75–79.
[34] A.J. Bard, L.R. Faulkner, Electrochemical Methods: Fundamentals and Applications, second ed., Wiley, New York, 2001.
[35] E. Laviron, Adsorption, autoinhibition and autocatalysis in polarography and in linear potential sweep voltammetry, J. Electroanal. Chem. 52 (1974) 355–393.
[36] M. Shap, M. Petersson, K. Edstrom, Preliminary determinations of electron transfer kinetics involving ferrocene covalently attached to a platinum surface, J. Electroanal. Chem. 95 (1979) 123–130.
[37] E. Laviron, General expression of the linear potential sweep voltammogram in the case of diffusionless electrochemical systems, J. Electroanal. Chem. 101 (1979) 19–28.
[38] H. Heli, N. Sattarahmady, A. Jabbari, A.A. Moosavi-Movahedi, G.H. Hakimelahi, F.Y. Tsai, Adsorption of human serum albumin onto glassy carbon surface-applied to albumin-modified electrode: mode of protein-ligand interactions, J. Electroanal. Chem. 610 (2007) 67.
[39] V. Brabec, DNA sensor for the determination of antitumor platinum compounds, Electrochim. Acta 45 (2000) 2929.
[40] X. Ju, Y.K. Ye, Y.L. Zhu, Interaction between nile blue and immobilized single- or double-stranded DNA and its application in electrochemical recognition, Electrochim. Acta 50 (2005) 1361–1367.
[41] S.S. Kalanur, U. Katrahalli, J. Seetharamappa, Electrochemical studies and spectroscopic investigations on the interaction of an anticancer drug with DNA and their analytical applications, J. Electroanal. Chem. 636 (2009) 93–100.
[42] B. Ojiha, G. Das, The interaction of 5-(Alkoxy)naphthalen-1-amine with bovine serum albumin and its effect on the conformation of protein, J. Phys. Chem. B 114 (2010) 3979–3986.
[43] D.M. Charbonneau, H.A. Tajmir-R.I.A.H.I, Study on the interaction of cationic lipids with bovine serum albumin, J. Phys. Chem. B 114 (2010) 1148–1155.
[44] J.R. Lakowicz, Principles of Fluorescence Spectroscopy, second ed., Plenum Press, New York, 1999.
[45] M.A. Khan, S. Muzammil, J. Musarrat, Interaction of genome-linked protein (VPg) of turnip mosaic virus with wheat germ translation initiation factors eIFiso4E and eIFiso4F, Int. J. Biol. Macramol. 30 (2002) 249.
[46] G. Sudlow, D.J. Birkett, D.N. Wade, Further characterization of specific drug binding sites on human serum albumin, Mol. Pharmacol. 12 (1976) 1052–1061.

[47] L. Stryer, R.P. Haugland, Energy transfer: a spectroscopic ruler, Proc. Natl. Acad. Sci. U. S. A. 58 (1967) 719–726.
[48] B. Valeur, J.C. Brochon, New Trends in Fluorescence Spectroscopy, third ed., Springer, Berlin, 2001.
[49] F.L. Cui, J. Fan, J.P. Li, Z.D. Hu, Interactions between 1-benzoyl-4-p-chlorophenyl thiosemicarbazide and serum albumin: investigation by fluorescence spectroscopy, Bioorg. Med. Chem. 12 (2004) 151–157.
[50] B. Valeur, Molecular Fluorescence: Principles and Applications, Wiley, New York, 2001.
[51] A. de Juan, A. Izquierdo-Ridorsa, R. Tauler, G. Fonrodona, E. Casassas, A soft-modeling approach to interpret thermodynamic and conformational transitions of polynucleotides, Biophys. J. 73 (1997) 2937–2948.
[52] J. Jaumot, R. Tauler, MCR-BANDS. A user friendly MATLAB program for the evaluation of rotation ambiguities in Multivariate Curve Resolution, Chemom. Intell. Lab. Syst. 103 (2010) 96–107.
[53] H. Abdollahi, R. Tauler, Uniqueness and rotation ambiguities in Multivariate Curve Resolution methods, Chemom. Intell. Lab. Syst. 108 (2011) 100–111.
[54] R. Tauler, Calculation of maximum and minimum band boundaries of feasible solutions for species profiles obtained by multivariate curve resolution, J. Chemom. 15 (2001) 627–646.
[55] H. Parastar, M. Jalali-Heravi, R. Tauler, Is independent component analysis appropriate for multivariate resolution in analytical chemistry? Trends Anal. Chem. 31 (2012) 134–143.
[56] R.M. Dyson, S. Kaderli, G.A. Lawrance, M. Maeder, A.D. Zuberbühler, Second order global analysis: the evaluation of series of spectrophotometric titrations for improved determination of equilibrium constants, Anal. Chim. Acta 353 (1997) 381–393.